International Journal of Microwave and Wireless Technologies

cambridge.org/mrf

Digital twin creation and residual analysis using CLEAN for radar target emulation

Arvid Sims[1], Bernhard Holzinger[1], Tom Vandeplas[2], Thomas Dallmann[3,4] and Dirk Heberling[5]

[1]Keysight Technologies Deutschland GmbH, Böblingen, Germany; [2]Keysight Technologies Belgium, Louvain, Belgium; [3]Funktechnologien für Automatisierte und Vernetzte Fahrzeuge, Technische Universität Ilmenau, Germany; [4]Industrielle Hochfrequenzsysteme, Fraunhofer-Institut für Hochfrequenzphysik und Radartechnik FHR, Germany and [5]Institute of High Frequency Technology, RWTH Aachen, Germany

Research Paper

Cite this article: Sims A, Holzinger B, Vandeplas T, Dallmann T, Heberling D (2026) Digital twin creation and residual analysis using CLEAN for radar target emulation. *International Journal of Microwave and Wireless Technologies*, 1–8. https://doi.org/10.1017/S1759078726103924

Received: 17 December 2025 UTC
Revised: 24 September 2026 UTC
Accepted: 27 September 2026 UTC

Keywords:
automotive radar; radar target simulator; radar target emulation; swerling; clean

Corresponding author: Arvid Sims; Email: arvid.sims@keysight.com

Abstract

Radar sensors in advanced driver assistance systems sense the traffic scene identifying reflections occurring in the environment. Clutter contained in the data is caused by multipath and scattering effects leading to signal processing challenges to identify weak targets, which is critical for vulnerable road users. To be able to test a radar for its robustness against clutter, suitable clutter models are required. In this paper, an approach for filtering reflections following the CLEAN algorithm is proposed. By iterative decomposition of processed radar data to a superposition of point sources, reflections are isolated for a replay with a radar target simulator (RTS) to form a digital twin. Field datasets recorded in a parking garage are analyzed for its radar target and clutter statistics. After the analysis, a list of possible point targets for replay with an RTS is available and residual radar cross-section levels are analyzed and compared to Swerling I case.

Introduction

Automotive radar applications include safety-relevant functions as emergency braking or adaptive cruise control. For a safe and reliable operation, traffic participants need to be identified with high fidelity. As radars transmit and receive electromagnetic waves, reflections resemble targets exhibiting a certain reflectivity. Transmitted electromagnetic waves propagate in the environment concluding in characteristic propagation paths, consisting of direct reflections and multipath behavior, which can be mapped to a certain driving environment. Frequency modulated continuous wave (FMCW) radars perform fast-Fourier transformations (FFTs) for computing range, velocity, and angle of arrival (AoA) information [1]. If the radar antenna gains are known, the radar cross-section (RCS) of targets can be estimated. Reflections with significant RCS can be further identified as traffic participants or infrastructure. A simplified block diagram of the processing chain is shown in Fig. 1.

Many sensors offer an output list of processed traffic objects which can be used for a replay with a radar target simulator (RTS) as digital twin [2, 3]. Additional information could still be extracted like scenario-specific clutter statistics. Especially the presence of clutter challenges the detection of vulnerable road users, and various methods are proposed to characterize [4, 5] and minimize its influence [6]. Recent research also investigates the clutter statistics of weather phenomenon like rain [7]. As consequence, a digital twin for the radar sensor should feature a model beyond the traffic participant list and include clutter statistics. In this paper, a method for analyzing ADC samples to determine clutter statistics and preparing the radar output for a playback with an RTS as digital twin is proposed. The approach is based on the CLEAN algorithm [8] and decomposes the range-Doppler (RD) map to a superposition of point targets. CLEAN was developed for radio astronomy but was adapted to radar processing to increase the deception capabilities of weak targets in the presence of strong ones [9]. For example, ground clutter was estimated and removed in passive radar application [10] and additional sidelobe suppression was investigated in pulse compression technique [11]. In this paper, CLEAN is applied to the RD map in FMCW-type radar for the automotive environment to compute a list of point targets. The identified targets are recorded and prepared for a replay in a laboratory using an RTS. Targets with a low RCS will be considered as clutter, the limit is set to a fixed RCS level in the algorithm. An earlier version of this paper was presented at the 22nd European Radar Conference (EuRAD) 2025 and was published in its proceedings [12]. In "Concept" section, the CLEAN method is presented and field data collection and applied processing is explained. In addition, the principle of RTS will be described. As extension to the previous publication,

© The Author(s), 2026. Published by Cambridge University Press in association with The European Microwave Association. This is an Open Access article, distributed under the terms of the Creative Commons Attribution-NonCommercial-NoDerivatives licence (http://creativecommons.org/licenses/by-nc-nd/4.0), which permits non-commercial re-use, distribution, and reproduction in any medium, provided that no alterations are made and the original article is properly cited. The written permission of Cambridge University Press or the rights holder(s) must be obtained prior to any commercial use and/or adaptation of the article.

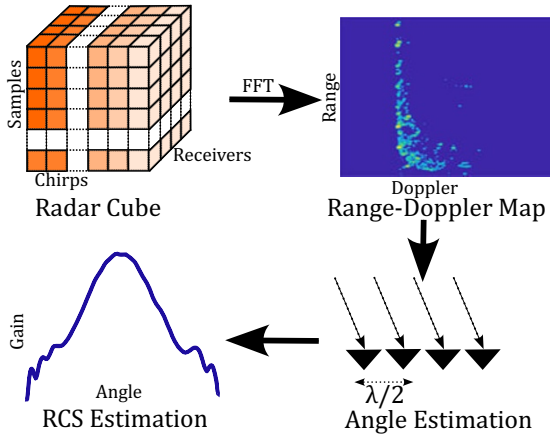


Figure 1. Typical signal processing chain in FMCW radar.

a second dataset is recorded and processed with CLEAN with improved handling of overlapping targets. Further analysis of the residual of the algorithm is performed. In "Data analysis using CLEAN" section, the algorithm for signal decomposition is applied and results are discussed. An interpretation of extracted clutter values for the scenario is provided and sensor effects influencing clutter statistics are identified. "Conclusion" section summarizes the results and proposes improvements and possible next steps.

Concept

Theoretical background

A common approach for isolating reflections leading to target detections are constant false alarm rate algorithms. They perform well against background noise and interference [13]. However, the approach of this paper is the recreation of the sensor receiver values including effects which may challenge the target detection of a radar. In order to form a digital twin of the radar data, the information is filtered using CLEAN. The goal is an approximation of the sensor receiver values with a limited set of point targets. CLEAN assumes the data can be described by a superposition of point sources which are affected by a point spread function (PSF). By decomposing the original data into a set of point sources and removing the PSF, a list of reflections is created which can be used as target list. Figure 2 describes the algorithm. The terminology assumes a "Dirty Map" or "Dirty Image" as initial dataset to be filtered. The Dirty Map is scanned for its maximum located in bin I. The peak multiplied by the PSF is considered the "Dirty Beam." The Dirty Beam is then subtracted and the residual becomes the "Residual Map" to be scanned for the next iteration. The algorithm continues until a defined threshold is reached.

Each RD map R can be sampled by a sum of weighted and shifted PSFs $A \cdot PSF(x - I)$ according to:

$$R = \sum_{i=1}^{k} \kappa \cdot A_i \cdot PSF(x - I_i) \tag{1}$$

κ is the loop gain and can be chosen to (0,1]. With a loop gain < 1, a reflection can be sampled by multiple smaller ones resulting in a better recreation of the signal. Especially sampling reflections from extended objects could be improved by this. As the number of available point reflections scales with hardware in an RTS, it is beneficial to synthesize the environment with the lowest amount of point targets. Therefore, a loop gain of $\kappa = 1$ is chosen. A scales the PSF with the amplitude of the measured peak.

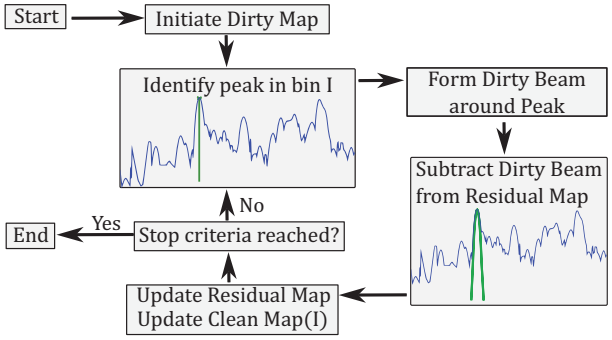


Figure 2. CLEAN algorithm flow chart.

Table 1. Radar parameters of dataset 1 and 2

Radar parameters	Value (AWR1642)	Value (AWR1843)
Start frequency	77 GHz	76 GHz
Range resolution	0.1526 m	0.2891 m
Doppler resolution	0.0919 m/s	0.0885 m/s
Radar cube	272 × 255 × 4	108 × 128 × 4
Stored sample width	16 bits	16 bits
Sampling rate	5.535 MSPS	12.5 MSPS
Measurement interval	500 ms	50 ms
RX channels	4	4
Field of view	±60°	±60°

Field data collection

Radar field data are recorded using an automotive radar evaluation kit TI AWR1642 with DCA1000 evaluation board mounted at the front of a car. While driving, analog-to-digital converter (ADC) values of the intermediate frequency signal are recorded. The collected data consist of radar cubes with 272 ADC samples, 255 chirps, and 4 receive channels. Every 500 ms, a new radar cube is fetched as radar snapshot. A total of 600 snapshots are recorded, resulting in a scenario duration of 5 minutes. For further analysis, a second dataset of the same environment is recorded with 5999 snapshots in the same time using the radar evaluation kit TI AWR1843. The datasets will be referred to as dataset 1 (AWR1642) and 2 (AWR1843). Parameters regarding the sensor configurations are summarized in Table 1.

As driving environment, a parking garage was chosen. The scenario is common in the automotive domain and features many large close-by scatterers like cars and metallic bars. Figure 3 shows a picture of the environment. The receiver noise floor is estimated by a background measurement against sky to avoid the measurement of any reflection. The mean and standard deviation s of the background data are calculated. Based on this, $3s$ environment around the mean noise level is excluded from the scenario data to ensure that noise will not contribute to the measurements. Furthermore, the field of view of the sensor is limited to ±60°. Data with wider estimated AoA are excluded.

https://doi.org/10.1017/S1759078726103924 Published online by Cambridge University Press

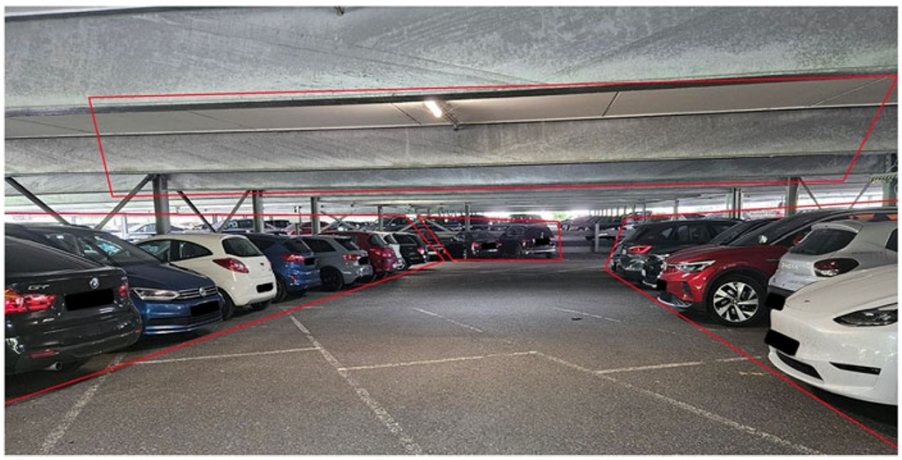
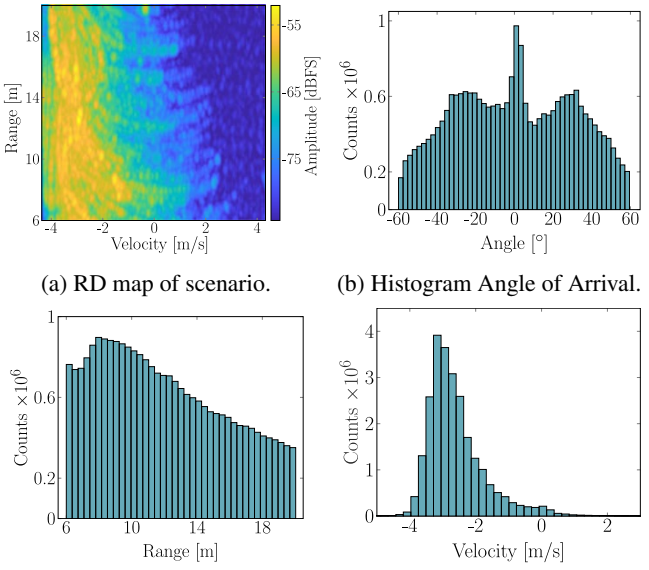


Figure 3. Parking garage as measurement environment.

ADC samples processing

The radar cube of each snapshot can be processed by applying an FFT. Its input data are multiplied by a Blackman window, zero-padding of factor 4 was applied. Reflections can be identified in the RD map. For AoA estimation, the Bartlett beamformer is used [13]. As output, receiver amplitudes normalized to the maximum and given in dBFS (decibels relative to maximum level or full scale) are available along range, Doppler, and AoA. Receiver values of the scenario are further regarded for the dataset 2 from TI AWR1843. Histograms of all values above the noise floor are summarized in Fig. 4 showing characteristic details about the environment and the applied processing. The vehicle was manually driven with a targeted speed around 10 km/h agreeing with 2.78 m/s. Due to manual driving and accelerating, the targeted speed can be slightly exceeded. The range from 6 to 20 m was further analyzed. An RD heat map shows maxima occurring in the scenario. It shows most reflections at the speed of the ego-vehicle and features angle-dependent Doppler migration effects from the detection of static objects and curve driving. The histogram of recorded velocities shows its peak at the measured negative ego-vehicle speed of −3.281 m/s and rolls off toward 0 m/s. The detected AoA histogram shows a maximum at 0°, which can be explained by the architecture of a garage forming a tunnel and reflecting energy back preferably at center axis. Obstacles along the driving way are present at all angles but appear dominantly as parking cars to the left and right. In addition, the sensor antenna pattern decreases toward larger angles resulting in fewer received values above the noise floor.

For simplification, the 2D RD map is compressed to a 1D range plot with the maximum receiver amplitudes across the Doppler dimension. Doppler shift is introduced by the only moving object of the scenario, which is the ego-vehicle itself. Furthermore, due to the compression and low antenna gain in the elevation plane, an AoA in the azimuth plane is assumed and each range bin in the 1D plot is associated with a single AoA. These simplified processing steps are expected to affect a target list and clutter statistics as, e.g., weak scatterers will be masked by stronger ones in a 1D plot. For converting the received values into RCS, a Keysight E8719A RTS is used. The received amplitude from the sensor is corrected against a reference target from the RTS. Any type of RTS or reference target with a fixed known RCS could be used. The gain pattern of the radar antenna is known; therefore, each AoA can be mapped to an antenna gain. The setup is shown in Fig. 5. By applying the radar equation [13], an RCS and the according received power for each range bin can be calculated.



(a) RD map of scenario. (b) Histogram Angle of Arrival. (c) Range histogram of detected bins. (d) Velocity histogram of detected bins.

Figure 4. Histograms of recorded scenario.

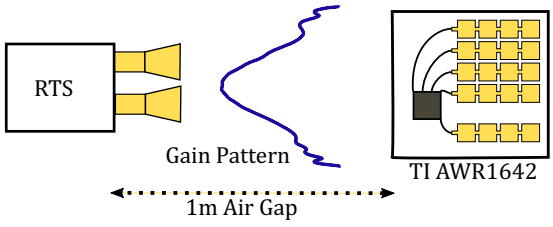


Figure 5. RCS correction factor measurement using an RTS.

Radar target emulation

An RTS modifies the radar signal emulating a fixed amount of point reflections with different delays, Doppler shifts, and amplitudes. This results in reported point targets with range, relative velocity and RCS [14]. Some architectures also allow the emulation of AoA [15, 16]. Advanced RTS solutions feature an arrangement of antennas similar to a screen allowing a multitude of point targets

https://doi.org/10.1017/S1759078726103924 Published online by Cambridge University Press

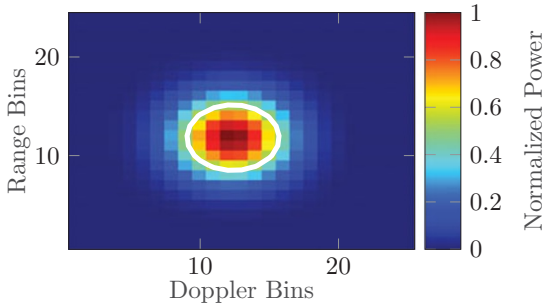


Figure 6. Measured and normalized point spread function with −3 dB contour.

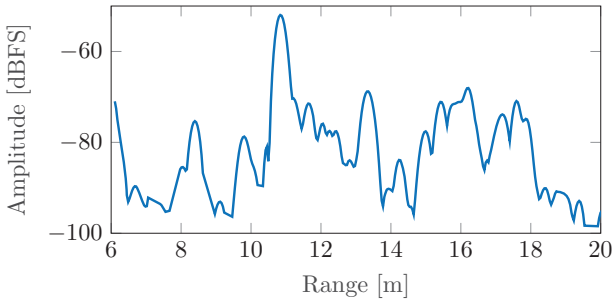


Figure 7. Snapshot range vs. amplitude in dBFS.

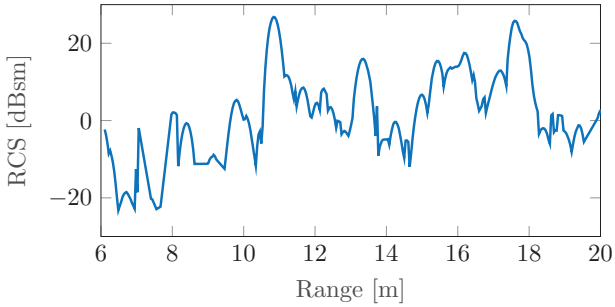


Figure 8. Snapshot range vs. RCS.

with multiple AoA, which can be utilized for playback of detection lists [17]. A final detection list always needs to be adapted to possible hardware limitations of the RTS, like, e.g., a maximum number of simultaneous targets [3]. For creating a digital twin from the sensor output data, it has to be mentioned that there is no standardized sensor output and recent research is discussing a possible metric to establish the objective validation of point cloud outputs [18]. The chosen approach aims to extract range, Doppler, RCS, and AoA information from the sensor for all received frames as these are parameters which can be set by an RTS and approximates sensor information by providing a set of scaled point reflections. An ideal point target has a constant RCS concentrated in a single RD map bin at a single AoA. This can be approximated with a corner reflector or point target being emulated by an RTS [19]. In the mathematical description of a propagation channel, an equivalent representation of a point target is the unit-impulse δ [20]. The processed output of a radar reporting a point target represents its system response. It includes radar-specific artifacts due to, e.g., antenna, windowing, and additional processing steps and can be used as PSF. A PSF for both datasets was measured, Fig. 6 shows the measured PSF of the TI AWR1642 in normalized power. Windowing (Blackman) was applied to reduce FFT sidelobes below the receiver noise floor. A PSF should be measured as high as possible above the noise floor ensuring scalability to various point target RCS sizes. Based on the radar configuration profile and the processing of ADC values, the PSF will change.

Data analysis using CLEAN

Target list extraction

After FFT processing, the RD map of each radar snapshot is available and compressed to a 1D range plot as described in "ADC samples processing" section. Its dBFS amplitude values are shown in Fig. 7. Peaks correspond to range bins and can include reflections from multiple AoA. The information can be converted in a range vs. RCS plot. Figure 8 shows RCS values according to the antenna gain at the estimated AoA. As only one dominant AoA is estimated per range bin, the curve may have discontinuities. It is used as Dirty Map for searching peaks according to Fig. 2. As iteration stop criterion for the parking garage scenario, an RCS level of 0 dBsm is set. An RCS of 0 dBsm is specified as typical value for a bicyclist as smaller traffic participant on the road [14]. The iteration stop criterion depends on the overall Signal-to-Noise Ratio of the analyzed scenario and is limited by the available dynamic range of the sensor. The iteration stop should be below the average scenario RCS for analyzing clutter statistics. For a sensor with higher dynamic range, a lower limit of −8 dBsm is proposed to include typical RCS of pedestrians [14] and thus to include all vulnerable road users. Table 2 summarizes the parameters used in the CLEAN algorithm, as well as those for radar processing. For creating a target list for an RTS with limited point targets per snapshot, a fixed number of targets can be set as stop criterion as well.

All snapshots are analyzed, a list of possible targets and the residual are recorded. Figure 9 shows the resulting superposition of point targets in RCS, up to the iteration stop of 0 dBsm, for a single range profile. Figure 10 shows the superposition of corresponding extracted PSF with respect to the iteration stop expressed in the originally received dBFS values. The iteration stop at 0 dBsm is converted into the corresponding dBFS values based on the estimated AoA. However, the list of targets for the digital twin needs to have a fixed AoA for each PSF. For the first dataset, CLEAN operates on reported magnitudes without phase information. A superposition of closely spaced overlapping targets is therefore considered with the same phase. The output of CLEAN shall be used as input for an RTS architecture. However, RTS architectures are not always able to offer the full control of the output phase, and an emulation of targets by RTS is often assumed to happen with random phases. As extension to the previous paper [12], the algorithm operates on reported power for the second dataset and assumes the incoherent superposition of radar targets. A full phase-coherent superposition is expected to yield the most realistic superposition of overlapping targets but requires phase information from the radar and phase control of the RTS architecture, which led to the decision of relying on an incoherent CLEAN implementation.

Residual analysis after CLEAN

All values below the iteration stop are considered clutter. These values are intended to be added as random fluctuating values in target emulation. The residual of CLEAN is defined by the iteration stop criterion. In this paper, the stop criterion is defined

https://doi.org/10.1017/S1759078726103924 Published online by Cambridge University Press

Table 2. CLEAN algorithm and radar processing parameters

Parameter	Dataset 1 and 2
Loop gain κ	1
Iteration stop criterion	0 dBsm residual map level
Zero-padding factor	4
Window	Blackman
PSF measurement method	RTS E8719A point target in RD map

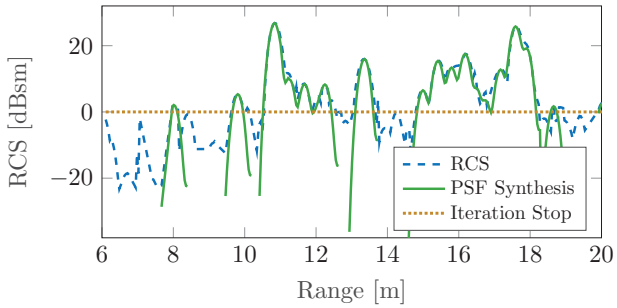


Figure 9. Snapshot range vs. RCS as superposition of point targets.

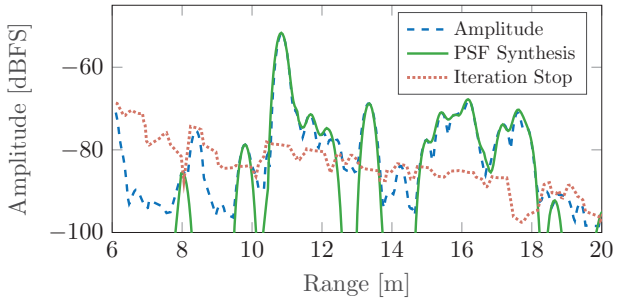


Figure 10. Snapshot range vs. amplitude recreated by weighted PSF.

with a fixed RCS value. Thus, the residual contains measured RCS values between the sensor detection threshold and the stop criterion of 0 dBsm. Stronger scattering centers are removed by CLEAN and the residual only shows low fluctuating echoes, which are expected to also originate from multipath. Its values are measured at different time snapshots and different ranges. To correctly interpret the residual statistics, both processing effects and sensor characteristics must be considered:

1) Range- and angle-dependent detectability:

Due to free-space path loss, targets with identical RCS are measured with different receive powers depending on their detected range. This results in a minimum detectable RCS that increases with target distance. Range-dependent detection effects are expected to bias the observed statistics and also affect the true RCS mean values of the environment. With a CLEAN iteration stop at 0 dBsm, the dynamic range of detectable clutter decreases with distance. At larger distances, fewer clutter samples can be observed, and only stronger residual contributions remain, as weaker scatterers fall below the minimum detectable RCS. Therefore, clutter statistics will also vary depending on analyzed range. An angle-dependent antenna gain further affects the minimum RCS by range to be detected at the boresight of the antenna only.

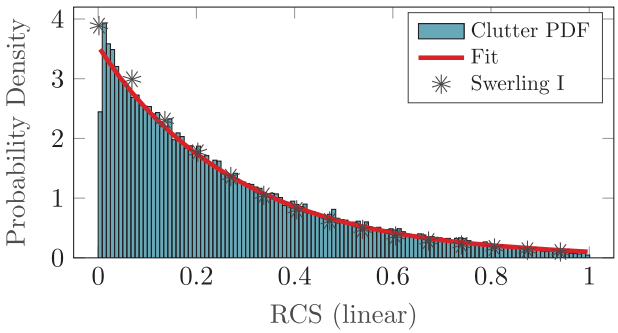


Figure 11. Histogram of residual (Dataset 1).

2) PSF-related and signal-processing effects:

Clutter contains the unfiltered residual content of the RD map and thus includes the target RCS roll-off from the PSF. It is therefore influenced by the scenario dynamics in range and time but also contains specific characteristics of the sensor itself. In addition, mathematical artifacts and imperfections of CLEAN can also contribute. The processing, FFT zero-padding, and compression of data influence statistics. Especially the simplified 1D compression can mask weak scattering centers, and a full 2D RCS estimation is expected to reveal a better model of the clutter statistics.

The environment can be considered as homogeneous due to a repeating driving path inside a parking garage. Due to the moving ego-vehicle, recorded reflections change their position each time snapshot. In order to analyze the fluctuation of clutter, a probability density function (PDF) of all received residual RCS can be calculated. The histogram in Fig. 11 shows the residual of the first dataset after CLEAN in RCS. The dataset was recalculated in this paper with improved angle estimation. By applying curve fitting, an exponential PDF can be associated with the histogram. The residual RCS values σ are showing an exponential behavior which resembles the fluctuating RCS of a Swerling I target [13]. This target model corresponds to a multitude of similarly large isotropic reflectors. From snapshot to snapshot, the composition and/or the position of the reflectors changes and so does the reported RCS. While the classical Swerling I model describes the snapshot-to-snapshot variation of an individual target, the observed behavior here results from an ensemble of weak, unresolved scattering contributions whose composition changes due to ego-vehicle movement. The exponential PDF therefore characterizes the aggregate fluctuation behavior of the residual clutter rather than that of a single physical target. In addition, the processed data include interpolated samples obtained via zero-padded FFT processing, which introduces correlations between adjacent bins and should therefore be regarded as oversampled representations of the same measurement rather than independent observations. This is expected to influence statistics and the true temporal scene mean. In Swerling I, the RCS is constant in a single snapshot but varies from snapshot to snapshot according to:

$$P(\sigma) = \frac{1}{\sigma_{avg}} \exp\left(-\frac{\sigma}{\sigma_{avg}}\right), \quad \sigma \geq 0 \tag{2}$$

with a mean RCS of σ_{avg}. A dataset mean RCS is calculated from all received residual clutter samples. In addition to that, extracted target lists from the scenario can also be analyzed for statistics in AoA, RCS, Doppler, and range for model creation of characteristic driving environments.

https://doi.org/10.1017/S1759078726103924 Published online by Cambridge University Press

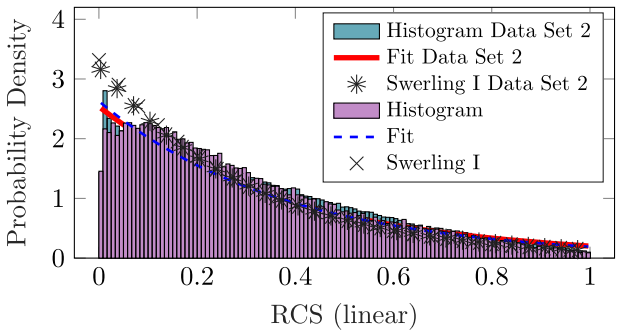


Figure 12. Histogram of residual for incoherent processing (Dataset 1 vs. Dataset 2).

As CLEAN operates without phase information, an incoherent superposition of overlapping targets is further assumed and CLEAN is performed again on both datasets. The histogram in Fig. 12 shows the residual of both datasets using incoherent subtraction in CLEAN. New effects in the PDF due to the changing physical interpretation of overlapping targets can be detected. Compared to Fig. 11, a larger mean residual RCS is observed. This behavior is expected, as incoherent subtraction of overlapping targets yields larger residual values than a subtraction in phase. The exponential fit exhibits a reduced matching, particularly at low RCS values, where the expected PDF peak is less pronounced. Both datasets show similar histogram shapes and mainly deviate at the exponential peak, which could be explained with improved and more sensitive measurement methods and slightly different sensor characteristics and antenna gains. The second dataset is therefore used for further analysis.

Limitations of residual analysis

Effects of a limited minimum detectable RCS mentioned in "Residual analysis after CLEAN" section will be analyzed in the following. By applying the radar equation, a minimum detectable RCS and the available dynamic range of clutter can be estimated. The clutter dynamics are limited by the RCS detection threshold and the iteration stop of 0 dBsm. Although the environment is considered to be homogeneous, this influences its radar perception. The clutter was separated into groups of smaller range patches which feature a change of the minimum detectable RCS with rising range of up to 3 dB. In addition, the angular field of view was limited to 3 dB beamwidth of the combined TX/RX antenna of the sensor. Thus, effects from range- and angle-dependent detectability were reduced, while still a large number of samples is available. The aggregated PDF of measured RCS across time snapshots can be calculated. Depending on range, a different amount of samples is available affecting the PDF. Especially at short ranges, clutter exhibits a larger dynamic range and a high number of measured samples. Figure 13 shows the corresponding PDFs with exponential fits, whose parameters were estimated by fitting the exponential function via nonlinear least-squares using the "fit" function of MATLAB ("Trust-Region" algorithm) with the initial value set to the samples mean. However, a matching of the fitted curve to the Swerling I model does not guarantee an exponential nature of the PDF, the deviation from the histogram can be observed. With rising range cells, migration of the PDF maximum is visible. This can be explained by the rising minimum detectable RCS imposed by the sensor noise floor rather than by the physical environment. Accordingly, the agreement with a Swerling I model evolves

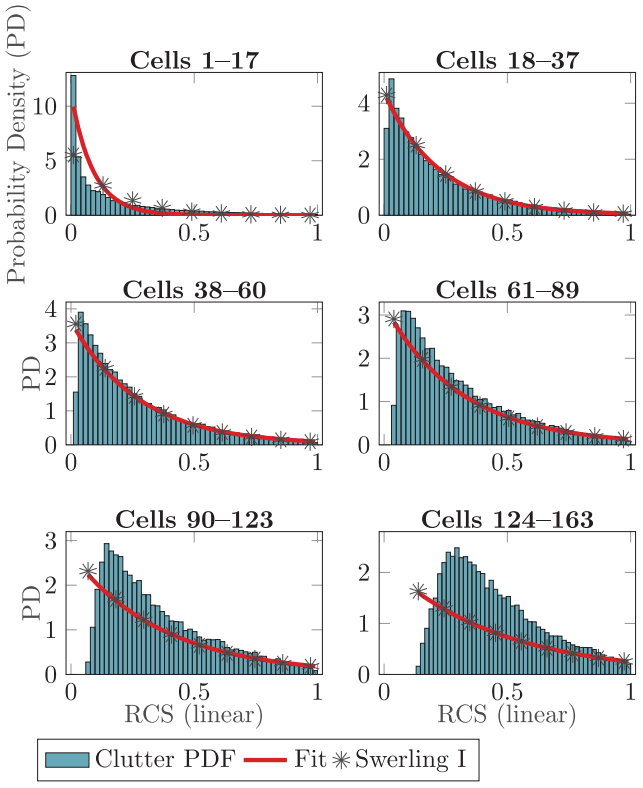


Figure 13. Histograms of multiple range patches.

from an overemphasized peak at short ranges to a good match at intermediate ranges and degrades clearly again at larger ranges. Interpolated samples are further expected to distort especially the PDF peaks. In addition, larger ranges also show fewer clutter detections; thus, fewer samples and are less suitable for statistical analysis. As example, the first PDF consists of 39,704 samples and features a dynamic range from 0 dBsm down to −24.55 dBsm for 6–7.15 m, the last PDF consists of 31,133 samples down to −5.74 dBsm for 14.88–17.7 m. In theory, Swerling I describes the fluctuation of a single target at a single range bin. But as scattering centers keep moving, even the analysis of a single range bin contains echoes from multiple migrating targets. For the analysis of the scenario clutter, it therefore makes no difference if adjacent range bins are pooled and thus form a global PDF of multiple equally scattering centers. But in addition, a sufficient and ideally equal dynamic range for clutter samples should be ensured for a statistical analysis. Thus, while the exponential behavior can resemble a Swerling I fluctuation model, the resulting PDF is shaped by the detection capability of the sensor rather than representing the properties of the of the environment alone. If the full scene over all ranges is pooled as a global PDF, the limited sample amount at larger distances contributes less to the statistics.

The findings show that sensor characteristics limit the perception of a cluttered scenario. Applying an exponential fluctuating model as Swerling I to resemble clutter appears to be a reasonable global model to emulate a more realistic clutter to target ratio. The sensor characteristics will shape the received clutter values for larger ranges by not displaying low exponential fluctuating values. However, the analysis also shows that sensor characteristics need to be considered while formulating clutter models to be used for emulation. It is recommended to consider this by analyzing smaller

https://doi.org/10.1017/S1759078726103924 Published online by Cambridge University Press

range patches with reduced angular coverage of similar antenna gain for local fluctuation models.

Conclusion

In this paper, a method for processing and preparing radar data for target simulators was proposed. By applying a PSF to each peak in the processed data, target lists were created as playback to form a digital twin. The quality of the digital twin depends on the processing of the field data. The accuracy of the digital twin is expected to improve by processing 2D RD maps and considering multiple AoA per detection in a range cell. Applying this, targets can be filtered at the same range with different Doppler shifts. With this approach, a traffic scene can be analyzed as targets lists of multiple snapshots are available and statistics of reported ranges, RCS, Doppler shifts, and AoA can be utilized. CLEAN can iterate to a threshold in RCS, while the lower boundary can be analyzed with a statistical approach. For the creation of a digital twin, the RTS hardware will be limited in the amount of point reflections and therefore fluctuating small reflections need to be emulated with a statistical approach. The data of low RCS fluctuations of the environment of the parking garage were compared with the Swerling I RCS target model. With extended analysis, sensor effects were shown and discussed regarding their influence on the clutter statistics. Local patches of fluctuating RCS were analyzed, and relevant factors as a changing detectable RCS and a limited dynamic range of clutter were discussed. As future steps, advanced CLEAN-based algorithms can be investigated, given that the original algorithm was introduced in 1974 and several method improvements have been proposed since then. Furthermore, more data from different traffic scenes can be collected and characteristic clutter models can be established. Additional work is required to further isolate clutter statistics from sensor and processing characteristics. The influence of the sensor position on the clutter statistics can be analyzed. In addition, the injection of a statistic approach into RTS hardware can be further investigated to enable the emulation of fluctuation loss with a clutter model.

Funding statement. This paper has been partially funded by the German Research Foundation (Deutsche Forschungsgemeinschaft, DFG) under grant 503852364.

Competing interests. The authors report no conflict of interest.

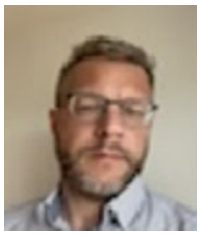
References

1. **Mafukidze H, Mishra A, Pidanic J and Francois S** (2022) Scattering centers to point clouds: A review of mmWave radars for non-radar-engineers. *IEEE Access* **10**, 110992 – 111021.
2. **Buddappagari S** (2021) Over-the-air vehicle-in-the-loop test system for installed-performance evaluation of automotive radar systems in a virtual environment. In *2020 17th European Radar Conference (EuRAD)*, Utrecht, Netherlands https://ieeexplore.ieee.org/document/9337434.
3. **Leon C, González-Huici M and Dallmann T** (2019) Data-driven generation of road scenarios for radar target simulation in automotive context. In *ICMIM 2019, IEEE MTT-S International Conference*, Detroit, MI, USA https://ieeexplore.ieee.org/document/8726648.
4. **Lee S, Lee B, Lee J, Sim H and Kim S** (2018) Iron tunnel recognition using statistical characteristics of received signals in automotive radar systems. In *19th International Radar Symposium (IRS)*, Bonn, Germany https://ieeexplore.ieee.org/document/8448246.
5. **Pandey N and Ram S** (2022) Characterization of millimeter wave clutter on Indian roads at automotive radar frequencies. In *International Conference on Radar Systems (RADAR 2022)*, Edinburgh, UK https://ieeexplore.ieee.org/document/10106297.
6. **Yoon J, Lee S, Lim S and Kim S** (2019) High-density clutter recognition and suppression for automotive radar systems. *IEEE Access* **7** 58368–58380.
7. **Gupta S, Varga I Hein M and Dallmann T** (2026) Analysis and empirical modeling of rain clutter for automotive radar validation. *International Journal of Microwave and Wireless Technologies* **18** Special Issue 3: EuCAP 2025 Special Issue, 401–408.
8. **Högbom J** (1974) Aperture synthesis with a non-regular distribution of interferometer baselines. *Astronomy and Astrophysics Supplement* **15**, 417–426.
9. **Kulpa K** (2008) The CLEAN type algorithms for radar signal processing. In *2008 Microwaves, Radar and Remote Sensing Symposium*, Kiev, Ukraine https://ieeexplore.ieee.org/document/4669567.
10. **Kulpa K *et al.*** (2019) CLEAN removal of ground clutter in mobile passive radar. In *2019 IEEE Radar Conference (RadarConf)*, Boston, MA, USA https://ieeexplore.ieee.org/document/8835846.
11. **He P, Chen B and Yang M** (2016) A novel sidelobe suppression method based on the CLEAN algorithm for bi-phase codes pulse compression. In *2016 CIE International Conference on Radar (RADAR)*, Guangzhou, China https://ieeexplore.ieee.org/document/8059434.
12. **Sims A, Holzinger B, Vandeplas T, Dallmann T and Heberling D** (2025) Digital twin creation using CLEAN for radar target emulation **1**. In *2025 22nd European Radar Conference (EuRAD)*, Utrecht, Netherlands, 35–38. 10.23919/EuRAD65285.2025.11234040.
13. **Gamba J** (2020) *Radar Signal Processing for Autonomous Driving*. : Singapore: Springer.
14. **ETSI TS 103 788** (2022) Short Range Devices (SRD) and Ultra Wide Band (UWB) measurement techniques and specifications for RX conformance tests with target simulator TS 103 788 https://www.etsi.org/deliver/etsi_ts/103700_103799/103788/01.01.01_60/ts_103788v010101p.pdf, Technical Specification, V1.1.1.
15. **Dallmann T, Mende J and Wald S** (2018) ATRIUM: A radar target simulator for complex traffic scenarios. In *2018 IEEE MTT-S International Conference on Microwaves for Intelligent Mobility (ICMIM)*, Munich, Germany https://ieeexplore.ieee.org/document/8443515.
16. **Real echoes in the lab - testing radar sensors with real radar echoes dSPACE Magazine** (2017) (2), 48–51.
17. **Holzinger B., Liebau H., Metzger M.**, Autonomous drive emulation methods and devices, Patent US 2021/0406562 A1, Dec. 30, 2021.
18. **Schmidt M, Widera A, Kahlert CTM and Bertram T** (2026) Point-to-point: Quantifying similarity in radar point clouds for automotive applications. In *2026 17th German Microwave Conference (GeMiC)*, Karlsruhe, Germany https://ieeexplore.ieee.org/document/11516418.
19. **Gowdu SJ, Asghar M, Nagel J, Rozmann M, Stephan R and Hein M** (2018) Comparison of real and simulated automotive radar targets measured with a reference radar. In *ICEAA*, Cartagena, Colombia.
20. **Sundararajan D** (2021) *Digital Signal Processing: An Introduction*, 1st ed. Cham, Switzerland: Springer.



Arvid Sims received a master in electrical engineering from RWTH Aachen University in 2019 and works for Keysight Technologies since then as application engineer for test & measurement solutions for automotive radar. His current work focuses on novel concepts for radar target emulation.

https://doi.org/10.1017/S1759078726103924 Published online by Cambridge University Press



Bernhard Holzinger is a Technical Architect at Automotive and Energy Solutions of Keysight Technologies. After joining Hewlett-Packard in 1995, he worked as an R&D engineer for more than 20 years participating on the development on measurement equipment for high-speed digital design. After joining Automotive and Energy Solutions in 2016, he is now focusing on two different areas. One is the improvement of measurement techniques to adapt the increasing speed of power electronics being based on wide bandgap technologies. In this context, he is a member of JEDEC WBG (Wide Band Gap) Working Group. The other area is the development of test solutions for ADAS and connected cars. He holds a BSEE from Berufsakademie Stuttgart with a focus on electronic and communications engineering.



Tom Vandeplas is a Senior Technical Architect at Keysight Technologies Laboratories. He began his career at Sirius Communications in 1999, working on satellite communication systems. After joining Agilent Technologies in 2001, he contributed to test and measurement systems with a focus on signal sources. Since 2008, when he joined Agilent Laboratories – now Keysight Laboratories – he has specialized in digital design and heterogeneous computing. His current work focuses on architecting scalable, integrated systems that enable next-generation test and measurement solutions. He holds an MSEE from Groep T Leuven with a focus on electronics and VLSI design.



Thomas Dallmann received the Dipl.-Ing. degree in electrical engineering from the RWTH Aachen University, Germany in 2010 and the Dr.-Ing. degree from the same institution in 2017. From 2016 to 2022, he was with the Fraunhofer-Institute for High Frequency Physics and Radar Techniques FHR, Wachtberg, Germany and lead a research group in Aachen, Germany. He is currently Junior Professor at Technische Universität Ilmenau, Germany, and responsible for the Radio Technologies for Automated and Connected Vehicles Research Group as well as the Electronic Measurements and Signal Processing Group. His research is concerned with integrated communication and sensing, radar sensing networks, and virtual validation of automotive radars.



Dirk Heberling (born August 15, 1961) (M'03-SM'10) studied electrical engineering and graduated with a Dipl.-Ing. degree from RWTH Aachen University, Aachen, Germany, in 1987. There he also received the Dr.-Ing. degree in 1993 for his thesis on conformal microstrip antennas. From 1987 to 1993, he was employed as a scientist at the Institute for RF-Technologies, RWTH Aachen University. In 1993, he joined IMST GmbH, Kamp-Lintfort, Germany, to establish a new Antenna Section and from 1995 to 2003 he was head of the Antennas Department, which was reorganized into the Department of Antennas and EMC in 1998. From 2003 to 2008, he took over the Department of Information and Communication Systems of IMST GmbH and in 2008 he moved to RWTH Aachen University where he is Head of the Institute and holder of the chair for High Frequency Technology. In addition, in 2016, he became director of the Fraunhofer Institute for High Frequency Physics and Radar Techniques, FHR.

https://doi.org/10.1017/S1759078726103924 Published online by Cambridge University Press